Towards the digital twin of a multi-stage forming process for metallic sheets

Nivesh Gautam, Tudor Balan, Francisco Chinesta, Sandrine Thuillier

Towards the digital twin of a multi-stage forming process for metallic sheets

NIVESH GAUTAM[a], TUDOR BALAN[b], FRANCISCO CHINESTA[c], SANDRINE THUILLIER[d]

a.Univ. Bretagne Sud, UMR CNRS 6027, IRDL, F-56100 Lorient, France
nivesh.gautam@univ-ubs.fr
b.Arts et Metiers Institute of Technology, Université de Lorraine, LCFC, Metz, France
tudor.balan@ensam.eu
c.Arts et Metiers Institute of Technology, PIMM & ESI Group chair, Paris, France
francisco.chinesta@ensam.eu
d.Univ. Bretagne Sud, UMR CNRS 6027, IRDL, F-56100 Lorient, France
sandrine.thuillier@univ-ubs.fr

Abstract :

Digital twins are a major constituent of advanced and smart manufacturing, to decrease the time to market, improve process efficiency and reduce waste production. There seems to be a common understanding on the different levels of integration of the communication between the physical object and the digital object, i.e., digital model, shadow and twin, with the digital twin being the stage when it sends actions to perform in real-time to the physical object, for an efficient execution of the process. In the field of material forming, digital models are well established nowadays, based on finite element simulations and physics-based constitutive equations to represent the material mechanical behavior, although in general the high calculation time prevents any real-time interaction. The aim of this study is to design first a digital shadow of a progressive multi-step sheet forming process, aiming at a digital twin in a second step. The target is to adjust the process parameters according to the mechanical properties variations. The physical process involves cutting of rectangular blanks, U-draw bending, springback and a last calibration stage to compensate for the springback. To provide a reliable representation of the mechanical behavior under complex stress states and large strains, distortional hardening is considered along with isotropic hardening. An analysis of variations of the mechanical properties of DP600 steel was performed, to generate several material parameter sets. Based on finite element simulations of the multi-step process, a sensitivity analysis of the forming process outputs to the mechanical properties variations is carried out. The results highlight the operating principle of the digital twin, stressing out the required sensors.

Keywords : multi-step forming process, sheet metal, U-draw bending, mechanical properties variations, digital twin

1 Introduction

One of the main challenges in deep drawing, which is a widely used cold forming process for sheet metals, is to produce parts without defects and corresponding to the geometrical specifications. All the more in the case of progressive sheet metal forming, where a flat metallic strip is fed into multiple successive stations, each station performing a forming operation at a given sequence and with a specific tooling [1]. This mass production technique is used to obtain complex structural components for automotive, aerospace and electronics industries [2]. Typical operations are punching [3], deep drawing [4], bending [5] and stamping [6]. Moreover, forming of a metallic sheet in multiple steps increases the formability [7] while also abetting geometrical compliance [8]. However, progressive forming requires a careful control of the process parameters, to save design time and improve the part quality [9], requiring a high number of trials to design the process [10, 11]. The issue of springback after the removal of the tools also becomes important concerning the involvement of different steps [12].

After the mechanical design stage, including tooling and process parameter definition, the variations of the material mechanical properties present an additional hurdle in progressive forming leading to inconsistent part quality, high rejection rates and the need for process parameter adjustments. Even within the same material class, mechanical properties can fluctuate due to the inevitable differences in the processing between batches [13], specially for dual phase steels with complex microstructure. Ultimately, changing the material batch has an influence on the forming process during industrial applications causing dimensional uncertainty [14]. Indeed, the formability of metallic sheets may depend on the original coil from which the blanks are cut, as evidenced for stainless steels [15]. The impact of uncertainties on material parameters for the flow stress, described by Swift's hardening law, on the hole expansion test of DP600 steel sheets was clearly highlighted [16]. It is therefore highly important to consider these influential variations so that the production performance and effectiveness can be enhanced.

Furthermore, advanced material models [17] are usually calibrated using the data from a single material batch, to develop a nominal model [18], yet are applied to make numerical predictions for several batches of the material, thereby introducing uncertainty in the numerical results. These nominal models, utilizing physics-based concepts and finite element (FE) simulations, provide reliable predictions of the forming process ultimately minimizing the cost and improving the performance. In order to make robust and accurate predictions, several physical phenomena need to be accounted for : metallic sheets undergo significant plastic deformation during the forming process and are subject to complex mechanical states leading to strain path changes [19] and non linear loading effects such as the Bauschinger effect and permanent softening [20]. Moreover, the multi-step forming process includes a high number of contacts between the sheet and tools and can lead to convergence issues while utilizing advanced material models [21].

Digital twin (DT) is a concept of Industry 4.0 that utilizes the physics based FE simulations along with data-driven concepts and smart algorithms [22] to further improve the efficiency of a manufacturing process [23]. DT was first defined by NASA [24] based on their Apollo space program and till date, the standard definition is still evolving. Based on a broad agreement, DT can be defined as the digital counterpart of a physical process with real time two-way synchronization of the data [25]. Application of DT in sheet metal forming are not very common, e.g., the digitalisation of a commercial sheet metal punching machine can be created with the help of 3D CAD models and simulation, exploiting the Ethernet/IP protocol for real time communication [26]. A similar use of 3D CAD model is repeated for the bending of sheet metal in V-shape [27], although the automated communication between the

physical and digital parts is not bilateral and it can be interpreted as a digital shadow [28]. Moreover, the digital twin may include regression models to determine process parameters for the physical process or material parameters, in the case of the drawing of cylindrical cups [29] and the front side of an automotive [30]. However, there is a still a lack of demonstrators, to apply in a practical way the whole concept [28], especially with multi-step forming process [18].

The main aim of this paper is to introduce a digital twin concept for progressive forming of metallic sheets, based on a nominal mechanical model corresponding to a real advanced high strength steel material. Section 2 presents the digital twin for the multi-step forming process, which involves springback compensation. In section 3, the mechanical model calibrated for a DP600 steel and the numerical model of the multi-step process are presented. Furthermore, variations of the mechanical properties are introduced within the supplier ranges and a sensitivity analysis on the part geometry and forming load is performed. These results are discussed in section 4, to highlight the digital twin operating principle, followed by concluding remarks in section 5.

2 Towards a digital twin for multi-step forming

The design of DT has been utilized in a vast category of studies and consistently been defined depending on the application. Typically, DT is developed for different phases of the product life cycle, namely design, production, service and retirement [31]. The present case is dedicated to the production phase, where the manufacturing of the real product takes place, to enhance the product quality and reduce material waste. Figure 1 illustrates the four pillars required to be defined for developing a successful DT [32]. A multi-step process is chosen and the final goal is to obtain a part with a given geometry, whatever the input parameters and in particular whatever the material batch.

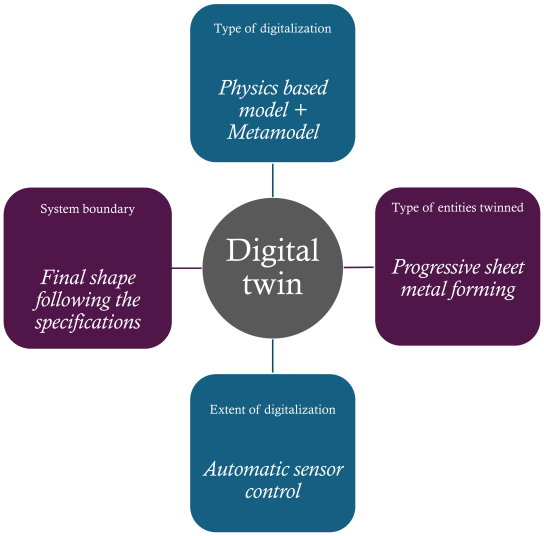

FIGURE 1 – Four pillars of a digital twin, i.e., type of entities twinned and system boundary, type and extent of digitalization [32], applied here to the multi-step forming process.

To further describe the digital twin, answers to the questions "What is digital ? What are we twinning" [32] are first presented.

2.1 What are we twinning ?

Figure 2 illustrates the digital twin developed for a progressive sheet metal forming process, highlighting the interaction between the physical object, or twin, and its virtual counterpart, to enable real time monitoring, response prediction and process optimization across multiple forming stages. The motivation of the forming process is driven by the importance of U-channels of metallic sheets which serve as critical components in automotive and aerospace engineering applications [33]. The U-draw bending process was used as a benchmark due to its industrially relevant forming conditions involving bending, drawing and non-monotonic loadings [34]. These conditions are very critical for calibration and validation of advanced material models [35], ultimately for the prediction of springback behavior, a key challenge in achieving the final part geometry. Indeed, in sheet metal forming, the final shape of the part is hampered by the undesirable elastic recovery, or springback, that occurs upon removing the forming tools. The magnitude of springback is highly sensitive to the material properties, sheet thickness and forming die geometries [36], blank holder force and die radius in case of stretch bending [37], punch velocity and bending radius in free bending [38], load holding time in V-bending [39]. FE simulations provide a better understanding of the mechanics of springback [40] and promote the reduction in manufacturing trial and error techniques by offering suitable modifications. Springback predictions are influenced by the choice of the yield criterion and strain hardening behavior under non linear loading conditions [41] as evidenced by the kinematic hardening [42] and distortional hardening approaches [43]. All the evidence from past studies indicates that the springback phenomenon in sheet metal forming can be adjusted by modifying the input process parameters to reach the final geometry, which is indeed the motivation for the development of the DT in the present study.

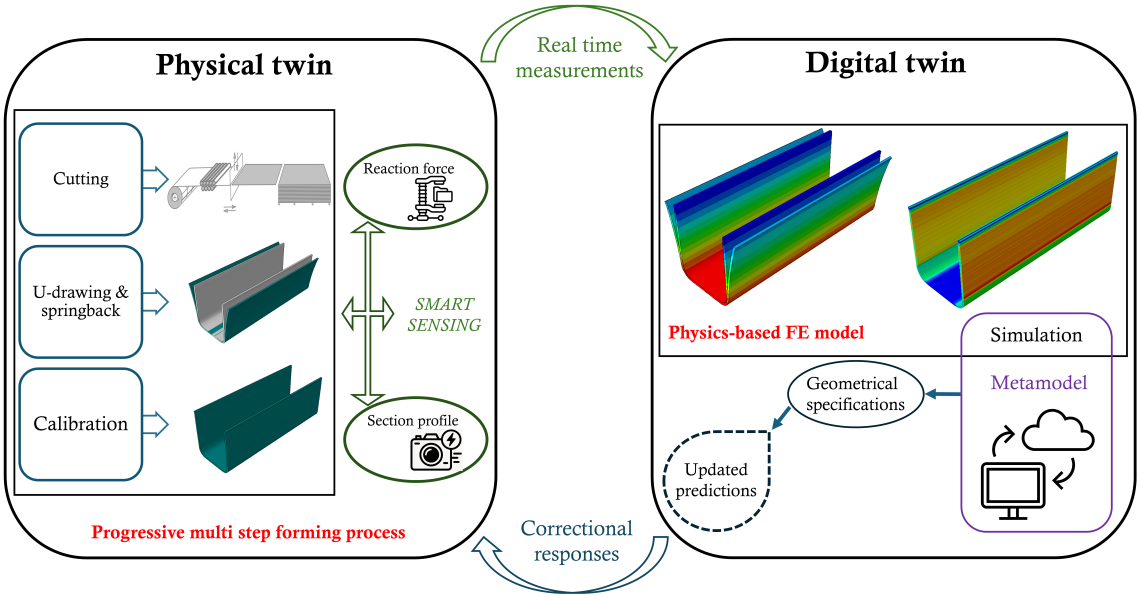

FIGURE 2 – Illustration of the digital twin concept for progressive sheet metal forming process developed in this study.

Over the years, many attempts have been made to minimize the springback in U-draw bending, e.g., by repeating the punch stroke to decrease the bending moment on the wall [44]. The reduction in bending moment can also be achieved by using a hollow punch and a counter stroke [45] or by utilizing bulgy bottoming process [46]. However, in the present context, the physical forming process include

3 progressive steps namely cutting of the square blank, U-draw bending, springback and a calibration step to compensate the springback, as illustrated in Figure 2. All the operations will be performed in a continuous and inline way, though the DT will deal only with the later 2 steps of the process, which are critical for the springback effects. The main goal of the this DT is to compensate the influence of mechanical properties on the springback magnitude and adjust the calibration step to always reach the same final part geometry.

2.2 What is digital ?

The digitalisation is based on finite element simulations using a physics-based mechanical model calibrated for a single material batch, further called the reference. In the context of DT, where real time interaction with the physical system is essential but full scale FE simulations are often too computationally intensive for direct integration, a Design of Experiments serves as a powerful method to sample limited yet representative simulation space. A metamodel, which can interpolate the behavior of full scale FE simulations with a significantly reduced computational effort, will be developed [18]. Figure 3 illustrates the flow chart of the forming process in the present study, highlighting the key input and output parameters involved in the process. The automated tensile testing will be performed in order to

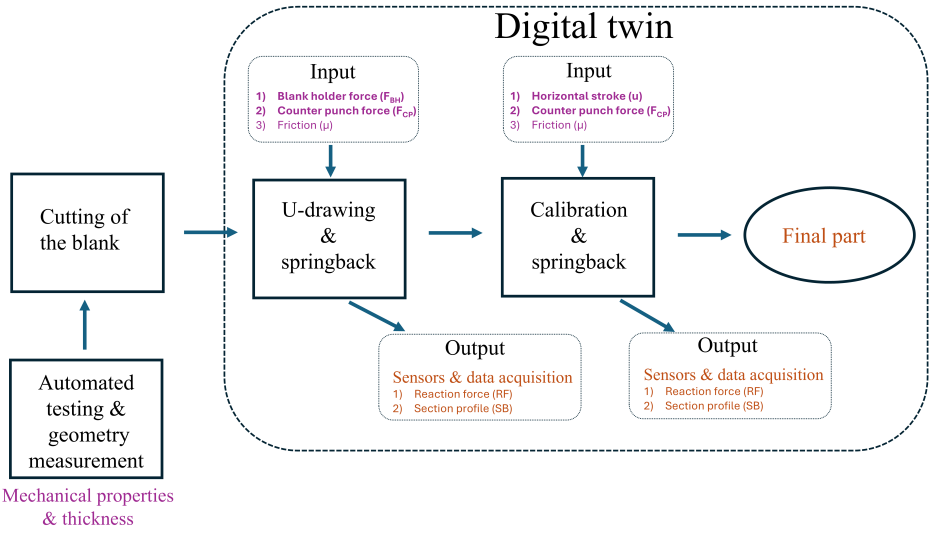

FIGURE 3 – A block diagram for the progressive sheet metal forming process. Input and output parameters are highlighted in violet and orange respectively. Input parameters that can be controlled with respect to the correctional response from the DT are highlighted in bold font.

characterize mechanical properties such as initial yield stress and ultimate tensile strength. And ultimately, from this knowledge, to control some process parameters to obtain the reference final shape of the part. A programmable logic controller (PLC) will receive information from physical sensors to control these process parameters. The data recorded from experiments are the reaction force of the tools and the section profile of the part. This data will be used to determine the horizontal stroke in the second step, so that the correctional response can be sent in real time to achieve the specified part geometry.

3 Nominal model and sensitivity analysis

3.1 Mechanical behavior of DP600

A dual phase steel DP600 of thickness $1.2\,\mathrm{mm}$, provided by ArcelorMittal, is considered in this study. The material's dual ferrite-martensite phase was revealed by scanning electron microscopy and the volume fraction of martensite was measured to be $14\% \pm 4\%$. The mechanical response at room temperature under quasi-static conditions was thoroughly characterized in uniaxial tension, hydraulic bulging and simple shear tests [21]. The shear tests included monotonic loading and non-monotonic loading sequences like a simple shear loading followed by unloading and then a reverse shear in the opposite direction. The mechanical properties and plastic anisotropy coefficients are calculated from tensile tests performed for 7 directions between rolling and transverse ones. It was found that : Young's modulus $E = 199\,\mathrm{GPa}$, initial yield stress $R_{p0.2} = 395\,\mathrm{MPa}$, ultimate tensile strength $R_m = 650\,\mathrm{MPa}$, normal and planar plastic anisotropy coefficients $\bar{r} = 0.99$ and $\Delta r = 0.09$ respectively. Initial anisotropy is neglected in this study.

3.2 Isotropic hardening

A combined Swift-Voce law is used to describe the isotropic hardening, defined as

$$\overline{\sigma}\left(\overline{\varepsilon}_p\right) = R\left[K\left(\varepsilon_0 + \overline{\varepsilon}_p\right)^n\right] + (1-R)\left[Q_1\left(1 - Q_2\exp\left(-Q_3\overline{\varepsilon}_p\right)\right)\right] \tag{1}$$

where $\overline{\varepsilon}_p$ is the equivalent plastic strain and $R, K, \varepsilon_0, n, Q_1, Q_2, Q_3$ are material parameters identified with the data from the tensile test in rolling direction and the bulge test, as illustrated in Figure 4a. The calibrated values of these parameters are presented in Table 2.

3.3 Distortional hardening

Homogeneous anisotropic hardening (HAH-2011) model is based on distortional hardening concept and developed as an alternative to kinematic hardening to represent the Bauschinger effect and permanent softening. The yield function of HAH-2011 model contains a stable ϕ and distortional ϕ_h part as defined in Equation 2.

$$\Phi(\mathbf{s}) = \left[\phi^q + \phi_h^q\right]^{\frac{1}{q}} = \left[\phi^q + f_1^q\left|\hat{\mathbf{h}} : \mathbf{s} - \left|\hat{\mathbf{h}} : \mathbf{s}\right|\right|^q + f_2^q\left|\hat{\mathbf{h}} : \mathbf{s} + \left|\hat{\mathbf{h}} : \mathbf{s}\right|\right|^q\right]^{\frac{1}{q}} = \overline{\sigma}(\overline{\varepsilon}_p) \tag{2}$$

Hybrid Swift-Voce law is used to describe the reference flow stress $\overline{\sigma}\left(\overline{\varepsilon}_p\right)$, and von Mises criterion is chosen. The distortional part is a function of the deviatoric stress $\mathbf{s}$, a tensorial internal variable $\mathbf{h}$, also called microstructure deviator and state variables f_1 and f_2. The microstruture deviator is defined as a normalized deviatoric tensor $\hat{\mathbf{h}}$

$$\hat{\mathbf{h}} = \frac{h_{ij}}{\sqrt{\frac{8}{3}h_{kl}h_{kl}}} \tag{3}$$

At the first plastic increment, the deviatoric stress tensor $\mathbf{s}$ is projected on the microstructure deviator and kept unchanged as long as the loading direction is the same. To quantify the magnitude of the strain path change, a parameter $\cos\chi$ is defined in a similar way to the strain-based one proposed in [47] but with a stress-based definition :

$$\cos\chi = \frac{8}{3}\hat{\mathbf{s}} : \hat{\mathbf{h}} \tag{4}$$

This parameter is equal to 1 for monotonic loading, -1 for reverse loading and 0 for cross loading. When the loading direction changes, the evolution of $\hat{\mathbf{h}}$ takes place as follows

If $\mathbf{s} : \hat{\mathbf{h}} \geq 0$

$$\frac{d\hat{\mathbf{h}}}{d\bar{\varepsilon}_p} = k\left[\hat{\mathbf{s}} - \frac{8}{3}\hat{\mathbf{h}}\left(\mathbf{s} : \hat{\mathbf{h}}\right)\right] \tag{5}$$

If $\mathbf{s} : \hat{\mathbf{h}} < 0$

$$\frac{d\hat{\mathbf{h}}}{d\bar{\varepsilon}_p} = k\left[-\hat{\mathbf{s}} + \frac{8}{3}\hat{\mathbf{h}}\left(\mathbf{s} : \hat{\mathbf{h}}\right)\right] \tag{6}$$

State variables f_1 and f_2 in Equation 2 are function of two other state variables g_1 and g_2, which physically represents the ratio of present flow stress to that of theoretical isotropic hardening one, defined as

$$f_k = \left[\left(\frac{1}{g_k} - 1\right)\right]^{\frac{1}{q}} \tag{7}$$

where $k = 1, 2$. State variables g_1 and g_2 are related to the Bauschinger effect and two additional variables g_3 and g_4 are introduced for permanent softening. Evolution laws for these 4 variables are defined as

If $\mathbf{s} : \hat{\mathbf{h}} \geq 0$

$$\frac{dg_1}{d\bar{\varepsilon}_p} = k_2\left(k_3\frac{\overline{\sigma}_0}{\overline{\sigma}(\bar{\varepsilon}_p)} - g_1\right) \tag{8}$$

$$\frac{dg_2}{d\bar{\varepsilon}_p} = k_1\frac{g_3 - g_2}{g_2} \tag{9}$$

$$\frac{dg_4}{d\bar{\varepsilon}_p} = k_5(k_4 - g_4) \tag{10}$$

If $\mathbf{s} : \hat{\mathbf{h}} < 0$

$$\frac{dg_1}{d\bar{\varepsilon}_p} = k_1\frac{g_4 - g_1}{g_1} \tag{11}$$

$$\frac{dg_2}{d\bar{\varepsilon}_p} = k_2\left(k_3\frac{\overline{\sigma}_0}{\overline{\sigma}(\bar{\varepsilon}_p)} - g_2\right) \tag{12}$$

$$\frac{dg_3}{d\bar{\varepsilon}_p} = k_5(k_4 - g_3) \tag{13}$$

There is a total of 6 parameters, which were identified using forward-reverse shear tests with two values of forward shear strain, i.e., 0.084 and 0.212. The calibrated values of these parameters are listed in Table 2. Figure 4b presents the prediction obtained with the identified parameters of HAH-2011 model as compared to experimental results.

3.4 Variations in mechanical properties

DP600 steel exhibits sensitive variations in the mechanical properties, primarily arising from the heterogeneous microstructural composition and the processing history of the sheets. In the present study, the calibrated values for isotropic hardening (HSV) model have been used as a reference and different hardening behavior have been generated. The standard range for initial yield stress and ultimate tensile strength are taken from ArcelorMittal catalogue [1]. This range was used for preparing different com-

1. https://automotive.arcelormittal.com/product_sheet

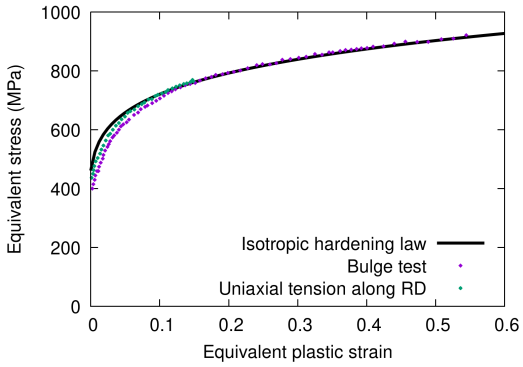

(a) Cauchy stress versus equivalent plastic strain for the different monotonic tests and the isotropic hardening law

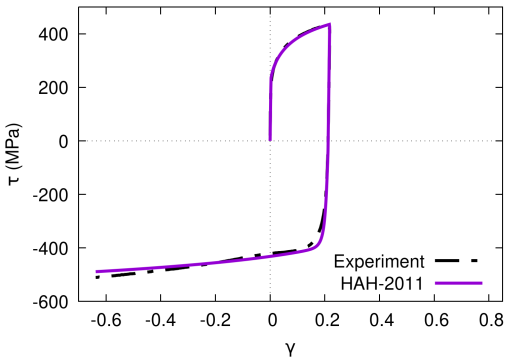

(b) Shear stress (τ) versus shear strain (γ) for the forward-reverse simple shear test and distortional hardening law

FIGURE 4 – Representation of the mechanical behavior of DP600 steel with HAH-2011, based on isotropic and distortional hardenings.

binations of initial yield stress and ultimate tensile strength, as listed in Table 1, leading to 3 sets of parameters for HSV model. Moreover, 2 sets of parameters for HAH-2011 model were arbitrarily generated; the hardening behavior is illustrated in Figures 5a and 5b. The values of the material parameters are shown in Table 2. The 2 parameter sets HSV-RF+HAH-SET1 and HSV-RF+HAH-SET2 give a si-

HSV SET	$R_{p0.2}$ (MPa)	R_m (MPa)	Combination
HSV-RF	395	650	Identified
HSV-SET1	330	593	$R_{p0.2}$ (Min), R_m (Min)
HSV-SET2	330	665	$R_{p0.2}$ (Min), R_m (Max)
HSV-SET3	430	695	$R_{p0.2}$ (Max), R_m (Max)

TABLE 1 – Combinations of initial yield stress and ultimate tensile strength for parameter sets

Set ↓ *HSV-Parameters* →	R	ε_0	K (MPa)	n	Q_1 (MPa)	Q_2	Q_3
HSV-RF	**0.8**	**0.0032**	**1060**	**0.175**	**756.4**	**0.437**	**26.05**
HSV-SET1	0.81	0.00325	863	0.179	716.3	0.414	26.04
HSV-SET2	0.589	0.0211	1473.94	0.397	770.19	0.499	27.06
HSV-SET3	0.795	0.00319	1165.21	0.173	778.66	0.446	25.84
Set ↓ *HAH-Parameters* →	k	k_1	k_2	k_3	k_4	k_5	-
HSV-RF+HAH-SET1	130	120	200	0.2	0.65	6.72	-
HSV-RF+HAH-SET2	**130**	**110**	**250**	**0.1**	**0.65**	**6.72**	-

TABLE 2 – Model coefficients of HSV (isotropic hardening) and HAH-2011 (distortional hardening) models for DP600. Calibrated values of the model coefficients are highlighted in bold. HSV-RF is taken as a reference model.

gnificant permanent softening, which relative magnitude, in absolute value, is respectively $16.8\,\%$ and $6.8\,\%$, compared to isotropic hardening (HSV-RF). The stress upon reloading is very similar for both sets, leading to a decrease by $17\,\%$ compared to isotropic hardening. Therefore, the investigated effect is related to permanent softening.

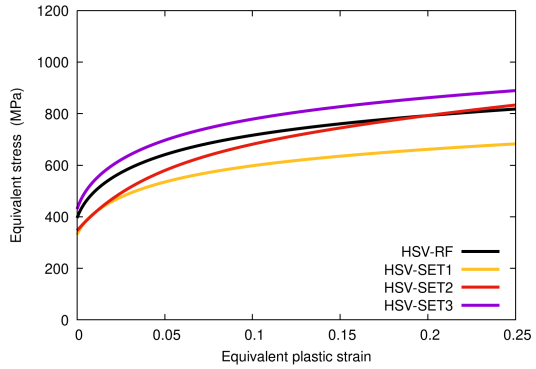

(a) Cauchy stress versus equivalent plastic strain for the different sets of parameters for the isotropic hardening law

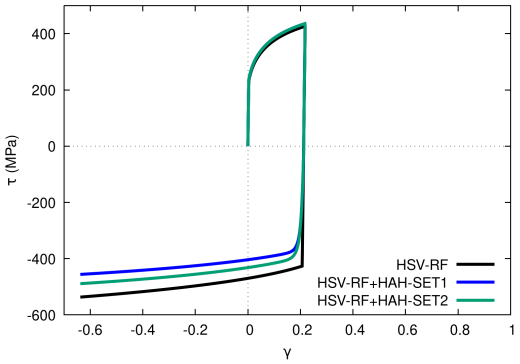

(b) Shear stress (τ) versus shear strain (γ) from forward-reverse simple shear test for different sets of distortional hardening law

FIGURE 5 – Variations in the mechanical behavior of DP600 steel

3.5 Forming process and numerical model

The forming process involves 2 stages, namely the U-draw bending and a calibration step of second bending for compensating the springback, with a tapered tool controlled by its horizontal stroke. The dimensions of the tools for both stages are given in Figure 6. FE analyses were carried out using ABAQUS version 2022 software. U-draw bending and second bending simulations were performed using the implicit and explicit solvers, respectively, while the springback analysis after each forming step was performed using the implicit solver. Indeed, simulation for the second bending stage with implicit solver unveils solution convergence issues and for this reason explicit solver was utilized. The HAH-2011 model along with a non-iterative stress update algorithms were implemented using user subroutines for implicit and explicit solvers [48].

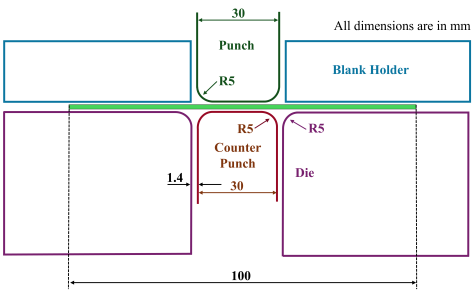

(a) U-draw bending stage

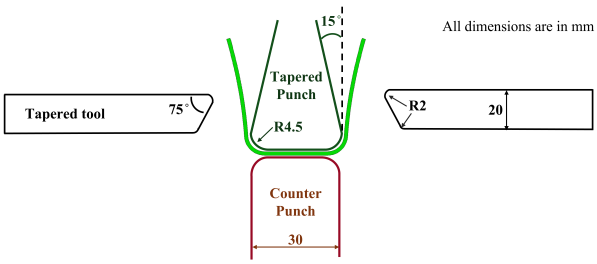

(b) Second bending stage

FIGURE 6 – Tool dimensions for the multistage process (in mm)

The original blank dimensions are $100\,\mathrm{mm} \times 100\,\mathrm{mm}$ and a quarter of the blank geometry was modeled considering the process symmetry, as illustrated in Figure 7. A mesh sensitivity analysis with mesh sizes of $1\,\mathrm{mm}$, $0.75\,\mathrm{mm}$ and $0.5\,\mathrm{mm}$ was performed, by analyzing the influence on the load and the final shape. The stress and strain distributions obtained from the U-drawing simulations utilizing explicit solver with mesh sizes of $0.75\,\mathrm{mm}$ and $0.5\,\mathrm{mm}$ were nearly identical, confirming mesh convergence. However, simulations of the U-drawing process with implicit solver with mesh sizes of $0.75\,\mathrm{mm}$ has solution convergence issues. For this reason, the blank was discretized using shell elements with reduced integration (S4R) of size 0.5 mm with 5 integration points in the thickness. Die and blank holder

were modeled as discrete rigid to apply the contact properties, so that the blank holder force can be removed once the blank leaves the space between these two tools and all the other tools are defined as analytical rigid surfaces. For the contact between the tools and the blank, the Coulomb friction law was used with a constant coefficient of 0.15. The blank holder force in U-draw bending step was $20\,\mathrm{kN}$ and counter punch force was set to $2\,\mathrm{kN}$ for both stages for the full blank dimensions. The punch stroke in the drawing step was $46\,\mathrm{mm}$ and a $9\,\mathrm{mm}$ horizontal stroke was applied on the tapered tool in order to perform the second bending step.

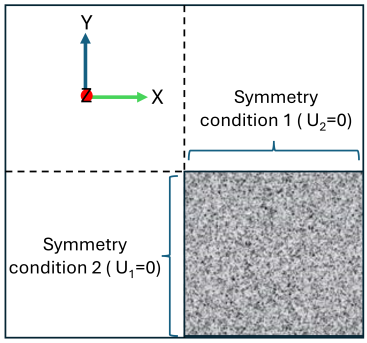

FIGURE 7 – Boundary conditions for a quarter of the blank (shaded area was simulated). U_1,U_2 and U_3 represents the displacement in X,Y and Z directions respectively.

3.6 Numerical results

The simulations were performed with isotropic hardening law (HSV) and a combination of isotropic and distortional hardening law (HSV+HAH). Figure 8 shows the reaction force of the punch in U-draw step and tapered tool in the second bending step. The small-amplitude oscillations in punch force are likely due to the contact changes and mesh effects, which are common in implicit simulations as the solver attempts to maintain equilibrium at each increment. Regarding the reaction force evolution of the tapered tool in the second bending stage, the first peak in the curves highlights the change in the contact points between the tapered tool and the blank wall as the horizontal stroke progresses. For the reference set of parameters, the maximum force level of the punch in U-draw bending and tapered tool in second bending is $36\,\mathrm{kN}$ and $1.1\,\mathrm{kN}$ respectively. It can be observed from the plot that the evolution of the reaction force is similar for all parameter sets, for both stages, though variations in mechanical properties influence the maximum load levels. The differences in the maximum load levels of the punch are higher than those of the tapered tool. It can also be observed that there is a slight difference in the prediction of the maximum load level by HSV-RF and HSV-RF+HAH-SET2 parameters, highlighting the influence of strain path changes.

Section profiles of the deformed blank,output in the middle of the blank, obtained from different sets of material parameters are shown in Figure 9. The plot compares section profile after U-draw bending (AF) and after springback, for both forming stages. For the U-draw bending step, it is very clear that the springback magnitude predicted by the reference parameter sets HSV-RF and HSV-RF+HAH-SET2 is very similar, i.e., taking account of the Bauschinger effect does not influence significantly the final shape. For the second bending step, the profiles suggest that the springback effects can be reduced by performing the second bending step.

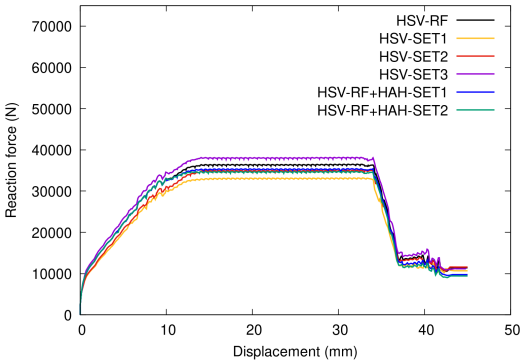

(a) Punch reaction force in U-draw bending

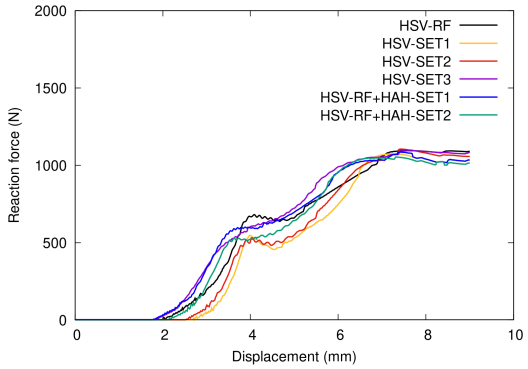

(b) Tapered tool reaction force in second bending

FIGURE 8 – Evaluation of reaction forces on tools during the 2 successive forming operations.

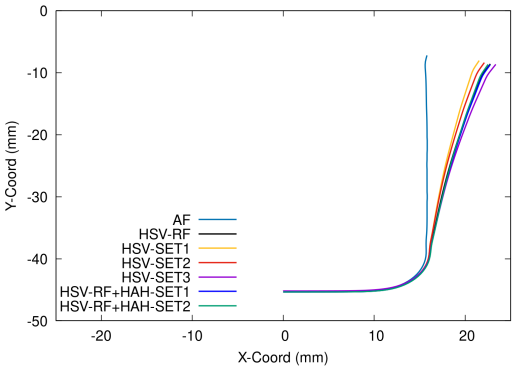

(a) Springback after U-draw bending

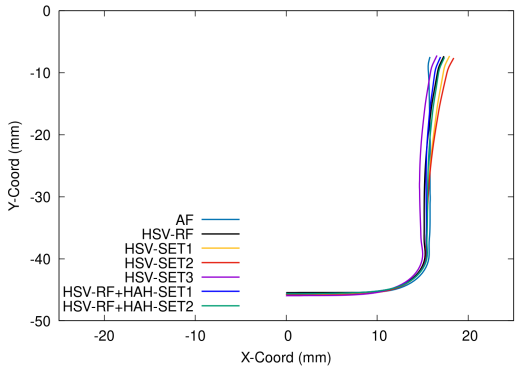

(b) Springback after second bending

FIGURE 9 – Section profile of the blank after forming operations and springback

4 Discussion

4.1 Sensitivity analysis of the variations in mechanical properties

Influence of variations in mechanical properties can be observed in the reaction force evolution and section profiles for U-draw bending and second bending step. In order to quantify the springback magnitude, the horizontal distance between the top extreme points of the wall after forming and after springback is computed. Figures 10 and 11 present the sensitivity of the maximum reaction force level of the moving tools and the springback distance with respect to the combinations listed in Table 1 in U-draw bending and second bending stage respectively. The best fit trend from these 3 combinations for U-draw bending stage shows that both the reaction force of the punch and magnitude of springback increase with the increase in $R_{p0.2}$ and R_m. Similarly, in the second bending stage, the reaction force level of the tapered tool can be seen increasing very slightly with the increase of $R_{p0.2}$ and R_m ; however, the springback magnitude decreases. The reason for the increase in load levels can be explained by the yield stress level : the higher it is, the higher the forming load. Concerning the reduction in the springback magnitude after the second bending step, the amount of overbending is higher for the large values of $R_{p0.2}$ and R_m, e.g., parameter set HSV-SET3, because the tapered tool comes in contact with the wall earlier than for the other sets of parameters, e.g., the point of contact for HSV-SET3 is at $1.78\,\mathrm{mm}$ and for HSV-SET1 is at $2.72\,\mathrm{mm}$ of tool displacement. And this earlier contact increases the second bending amount thereby reducing the springback by a high margin compared to the other sets.

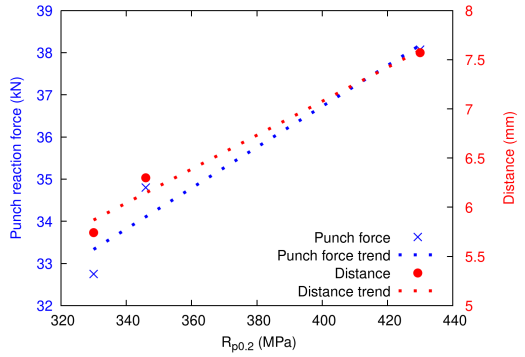

(a) Sensitivity to initial yield stress

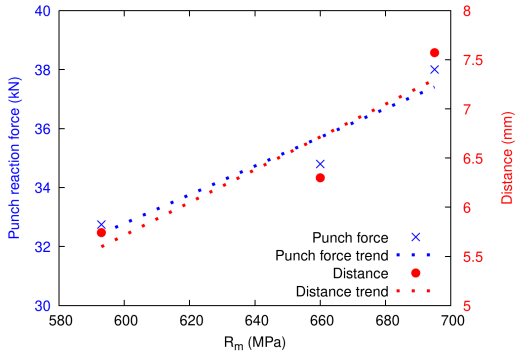

(b) Sensitivity to ultimate tensile strength

FIGURE 10 – Effect of initial yield stress and ultimate tensile strength on reaction force level of punch and springback distance in U-draw bending stage

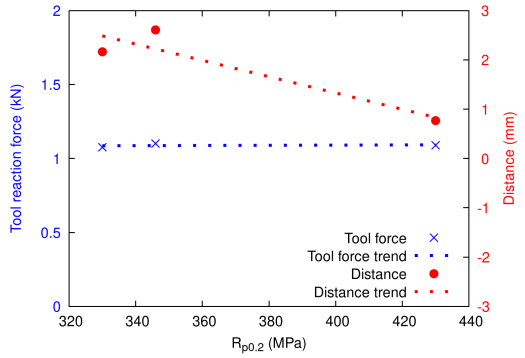

(a) Sensitivity to initial yield stress

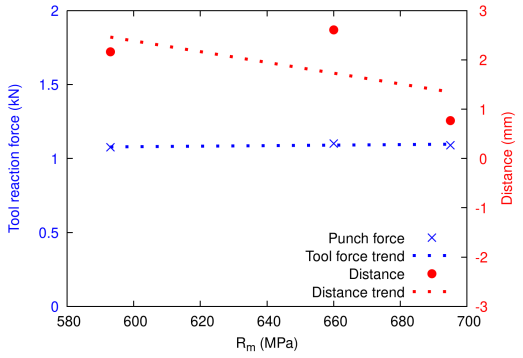

(b) Sensitivity to ultimate tensile strength

FIGURE 11 – Effect of initial yield stress and ultimate tensile strength on reaction force level of horizontal tool and springback in second bending stage

Regarding the virtual predictions obtained with the 2 sets of HAH model parameters, the reaction force level of the tools exhibits sensitive differences, though the springback distance is very close to the prediction obtained with the reference set (HSV-RF). Figure 12 shows the effect of a change in hardening level in the reverse direction, often referred to as permanent softening, on the load level and springback distance for both forming stages. It can be seen from the trend that the reaction force and springback magnitude increase as the permanent softening decreases however, the change is very small in springback distance. Multiple studies have shown that distortional plasticity models (e.g., extension of HAH-2011 used in this study) and isotropic hardening models can yield nearly identical springback predictions. Wiper bending simulation involving 3 bending steps with two direction reversals interestingly shows minimal differences in terms of springback prediction between isotropic hardening and distortional hardening for the second bending stage [49]. Identical prediction of springback from isotropic and HAH models was also observed in roll forming of martensitic advanced high-strength steels [50] and in U-draw bending of DP780 steel [51] and aluminum alloys of 7xxx series [52]. In the present study, reverse strain path change is predominant and it tends to minimize the residual torque, ultimately reducing the springback regardless of the amount of Bauschinger effect in play [50].

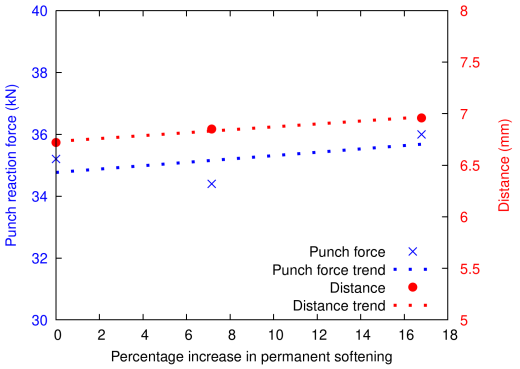

(a) Effect on U-draw bending stage

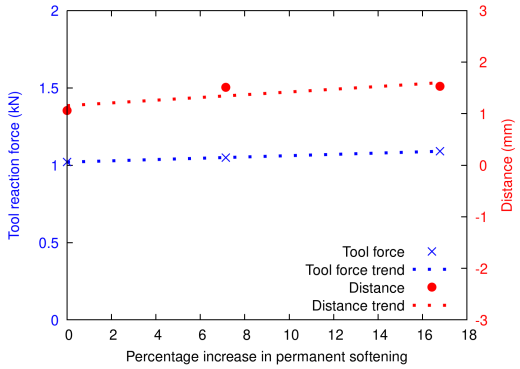

(b) Effect on second bending stage

FIGURE 12 – Effect of change in reverse hardening behavior with the help of HAH parameters on reaction force level and springback distance in both forming stages. HSV-RF has no permanent softening, whereas HSV-RF+HAH-SET2 leads to a relative increase of permanent softening of $6.8\,\%$ and HSV-RF+HAH-SET1 of $16.8\,\%$.

4.2 Illustration of DT in operation

Concerning the DT, the main target is to obtain a given final shape, by adjusting the tapered tool horizontal displacement. With a constant value of $9\,\mathrm{mm}$, it was shown that the final shape depends on the mechanical properties. Additional numerical simulations, with 2 other values for the horizontal stroke, i.e., $10\,\mathrm{mm}$ and $11\,\mathrm{mm}$, for HSV-SET1, were performed, to highlight the functioning of the DT. Indeed, HSV-SET1 does not give the reference shape and the horizontal stroke should be adjusted by the DT. Figure 13 presents the section profile and the trend for springback magnitude reduction obtained with the 3 values for the horizontal stroke. It can be observed that the springback distance can be modified by changing the horizontal stroke value in order to achieve the final reference shape. A change of mechanical properties corresponding to HSV-SET1 should be compensated automatically by the DT by adjusting the horizontal stroke to $9.46\,\mathrm{mm}$. The metamodel will be constructed based on a design of experiments that accounts for both the material's mechanical properties and the forming process parameters, although the specific methodology has yet to be determined [53].

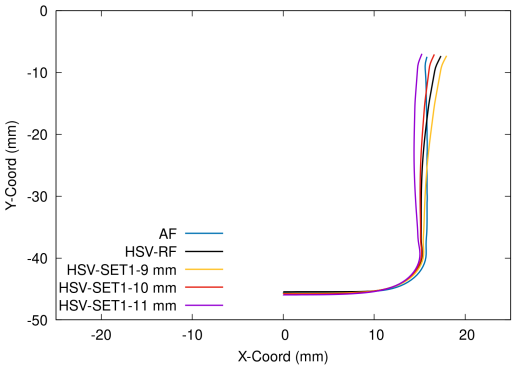

(a) Effect on section profile

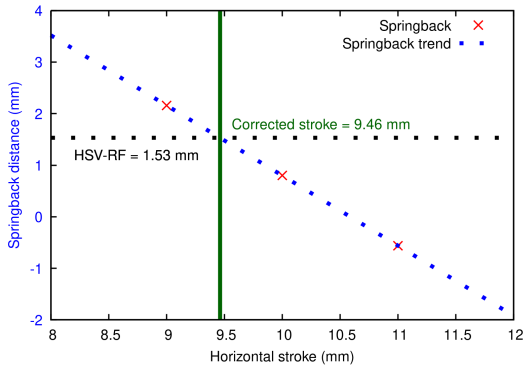

(b) Illustration of springback trend

FIGURE 13 – Illustration of reduction in springback distance through variations in horizontal stroke for HSV-SET1. The horizontal line stands for the reference target value to achieve. Intersection point of the reference target value and springback trend-line is highlighted with the help of green vertical line which corresponds to the corrected stroke required for acquiring the final target shape.

5 Conclusions

A study was conducted with two main objectives : to define a digital twin for a multi-step forming process of metallic sheets and to illustrate how this DT would work using a numerical nominal model and by introducing mechanical properties variations. Numerical simulations of a multi-step forming process consisting of a U-draw bending operation followed by a bending step were performed considering a DP600 steel and using isotropic hardening combined with a distortional hardening model. An analysis of the variations in mechanical properties of DP600 was also performed, in order to highlight their influence on the forming process. Based on the results obtained, the following conclusions can be drawn :

- a DT framework was defined for a progressive sheet metal forming process and its objectives are highlighted with the help of a numerical sensitivity analysis,
- variations in mechanical properties influence the reaction force as well as springback magnitude in U-draw bending. However, the effect is comparatively less in the second bending stage,
- springback magnitude after the U-draw bending process can be compensated by performing a subsequent bending step with the help of a tapered tool, controlled by its horizontal displacement (stroke),
- identical predictions for springback magnitude could be obtained for both isotropic hardening and advanced distortional hardening model in the forming process, though the reverse strain path change is dominant.

Acknowledgments

This project has received funding from the Research Fund for Coal and Steel under grant agreement No 888153 (project VForm-xSteels) and from Institut Carnot ARTS (project DAMAS).

Disclaimer
The results reflect only the authors' view, and the European Commission is not responsible for any use that may be made of the information it contains.

References

[1] Y. Gen, W. Yunong, Progressive stamping process and die design of high strength steel automobile structural parts, Journal of Physics: Conference Series, IOP Publishing, 2020, pp. 012063.

[2] D.A. Molitor, and A. Kokozinski, C. Kubik, V. Arne, C. Veitenheimer, F. Georgi, R. Krämer, P. Groche, Identifying productivity-limiting factors in progressive die stamping: data-driven methodology for process optimization, Production Engineering, 2025.

[3] R. Hambli, Metal flow prediction during sheet-metal punching process using the finite element method, The International Journal of Advanced Manufacturing Technology, 33 (2007) 1106–1113.

[4] A. Atrian, F. Fereshteh-Saniee, Deep drawing process of steel/brass laminated sheets, Composites Part B: Engineering, 47 (2013) 75–81.

[5] Y.E. Ling, H.P. Lee, B.T. Cheok, Finite element analysis of springback in L-bending of sheet metal, Journal of Materials Processing Technology, 168 (2005) 296–302.

[6] R. Sowerby, J.L. Duncan, E. Chu, The modelling of sheet metal stampings, International Journal of Mechanical Sciences, 28 (1986) 415–430.

[7] H.J. Bong, F. Barlat, J. Lee, M.G. Lee, J.H. Kim, Application of central composite design for optimization of two-stage forming process using ultra-thin ferritic stainless steel, Metals and Materials International, 22 (2016) 276–287.

[8] J. Imbert, M. Worswick, Electromagnetic reduction of a pre-formed radius on AA 5754 sheet, Journal of Materials Processing Technology, 211 (2011) 896–908.

[9] A. Lagroum, P.-Y. Manach, S. Thuillier, From single to multi-stage forming process of copper thin sheet, Mechanics & Industry, 26 (2025) 4.

[10] Y. Abe, K. Mori, O. Ebihara, Optimisation of the distribution of wall thickness in the multistage sheet metal forming of wheel disks, Journal of Materials Processing Technology, 125-126 (2002) 792–797.

[11] K. Mori, Y. Abe, Y. O. Ebihara, Prevention of shock lines in multi-stage sheet metal forming, International Journal of Machine Tools and Manufacture, 43 (2003) 1279–1285.

[12] W. Julsri, S. Suranuntchai, V. Uthaisangsuk, Finite element based analysis of two-stage forming for advanced high strength steel part, Procedia Manufacturing, 15 (2018) 668–675.

[13] G. Ouaidat, A. Lagroum, A. Kacem, S. Thuillier, Uncertainties on the mechanical behaviour of bronze sheets: influence on the failure in bending, International Journal of Material Forming, 17 (2024) 29.

[14] A. Weckenmann, M. Knauer, T. Killmaier, Uncertainty of coordinate measurements on sheet-metal parts in the automotive industry, Journal of Materials Processing Technology, 115 (2001) 9–13.

[15] V. Karthik, R.J. Comstock, D.L. Hershberger, R.H. Wagoner, Variability of sheet formability and formability testing, Journal of Materials Processing Technology, 121 (2002) 350–362.

[16] K. Prasad, D. Kumar, H. Krishnaswamy, D.K. Banerjee, Uncertainties in the Swift hardening law parameters and their influence on the flow stress and the hole expansion behavior of dual-phase (DP600) steel specimens, Journal of Materials Engineering and Performance, 32 (2023) 9206–9220.

[17] D. Hérault, S. Thuillier, S.-Y Lee, P.-Y. Manach, F. Barlat, Calibration of a strain path change model for a dual phase steel, International Journal of Mechanical Sciences, 194 (2021) 106217.

[18] V. Champaney, F. Chinesta, E. Cueto, Engineering empowered by physics-based and data-driven hybrid models: A methodological overview, International Journal of Material Forming, 15 (2022) 31.

[19] J.H. Schmitt, E.L. Shen, J.L. Raphanel, A parameter for measuring the magnitude of a change of strain path: Validation and comparison with experiments on low carbon steel, International Journal of Plasticity, 10 (1994) 535–551.

[20] N. Gautam, S. Yoon, F. Barlat, S. Thuillier, Comparison of homogeneous anisotropic hardening models in the case of the direct redrawing of a DP600 steel, IOP Conference Series: Materials Science and Engineering, IOP Publishing, 2024, pp. 012029.

[21] D. Herault, Virtual forming of metallic sheet materials : influence of complex strain paths on service life prediction, Thesis, University of South Brittany, 2021.

[22] F. Tao, Q. Qi, L. Wang, A.Y.C. Nee, Digital twins and cyber–physical systems toward smart manufacturing and industry 4.0: Correlation and comparison, Engineering, 5 (2019) 653–661.

[23] K.Y.H. Lim, P. Zheng, C.-H. Chen, A state-of-the-art survey of Digital Twin: techniques, engineering product lifecycle management and business innovation perspectives, Journal of Intelligent Manufacturing, 31 (2020) 1313–1337.

[24] M. Shafto, M. Conroy, R. Doyle, E. Glaessgen, C. Kemp, J. LeMoigne, L. Wang, Draft modeling, simulation, information technology & processing roadmap, Technology area, 11 (2010) 1–32.

[25] B. Schleich, N. Anwer, L. Mathieu, S. Wartzack, Shaping the digital twin for design and production engineering, CIRP annals, 66 (2017) 141–144.

[26] A. Moreno, G. Velez, A. Ardanza, I. Barandiaran, A.R. de Infante, R. Chopitea, Virtualisation process of a sheet metal punching machine within the Industry 4.0 vision, International Journal on Interactive Design and Manufacturing, 11 (2017) 365–373.

[27] E.P. Hinchy, C. Carcagno, N.P. O'Dowd, C.T. McCarthy, Using finite element analysis to develop a digital twin of a manufacturing bending operation, Procedia CIRP, 93 (2020) 568–574.

[28] W. Kritzinger, M. Karner, G. Traar, J. Henjes, W. Sihn, Digital Twin in manufacturing: A categorical literature review and classification, Ifac-PapersOnline, 51 (2018) 1016–1022.

[29] M. Ryser, P. Hora, M. Bambach, On the use of fixed point translations as input variable for digital twins in deep drawing compared to current methods, IOP Conference Series: Materials Science and Engineering, IOP Publishing, 2021, pp. 012084.

[30] M. Ryser, F.M. Neuhauser, C. Hein, P. Hora, M. Bambach, Surrogate model–based inverse parameter estimation in deep drawing using automatic knowledge acquisition, The International Journal of Advanced Manufacturing Technology, 117 (2021) 997–1013.

[31] M. Liu, S. Fang, H. Dong, C. Xu, Review of digital twin about concepts, technologies, and industrial applications, Journal of Manufacturing Systems, 58 (2021) 346–361.

[32] A. Agrawal and M. Fischer, What is digital and what are we twinning?: a conceptual model to make sense of digital twins,in Handbook of Digital Twins, CRC Press, Abingdon, 2024.

[33] O.M. Ikumapayi, E.T. Akinlabi, N. Madushele, S.O. Fatoba, A brief overview of bending operation in sheet metal forming, Advances in Manufacturing Engineering: Selected articles from ICMMPE 2019, Singapore, 2020, pp. 149–159.

[34] A. Makinouchi, E. Nakamachi, E. Onate, R.H. Wagoner, Numerical simulation of 3D sheet metal forming processes-Verification of simulation with experiment, Proceedings of the 2nd International Conference NUMISHEET'93, 1993.

[35] S.Y. Lee, S.Y. Yoon, J.H. Kim, F. Barlat, Calibration of distortional plasticity framework and application to U-draw bending simulations, ISIJ International, 60 (2021) 2927–2941.

[36] Z. Tekıner, An experimental study on the examination of springback of sheet metals with several thicknesses and properties in bending dies, Journal of materials processing technology, 145 (2004) 109–117.

[37] E.H. Ouakdi, R. Louahdi, D. Khirani, L. Tabourot, Evaluation of springback under the effect of holding force and die radius in a stretch bending test, Materials & Design, 35 (2012) 106–112.

[38] M. Krinninger, D. Opritescu, R. Golle, W. Volk, Experimental investigation of the influence of punch velocity on the springback behavior and the flat length in free bending, Procedia Cirp, 41 (2016) 1066–1071.

[39] M.A.H. Mithu, M.A. Karim, F.A. Taj, A. Rahman, Predicting springback in V-bending: Effects of load, load holding time, and heat treatment on common sheet-metal forming operations, Materials Today Communications, 43 (2025) 111668.

[40] K.P. Li, W.P. Carden, R.H. Wagoner, Simulation of springback, International Journal of Mechanical Sciences, 44 (2002) 103–122.

[41] J. Kim, W. Lee, D. Kim, J. Kong, C. Kim, M.L. Wenner, K. Chung, Effect of hardening laws and yield function types on spring-back simulations of dual-phase steel automotive sheets, Metals and Materials International, 12 (2006) 293–305.

[42] P.-A. Eggertsen, K. Mattiasson, On constitutive modeling for springback analysis, International Journal of Mechanical Sciences, 52 (2010) 804–818.

[43] J. Choi, J. Lee, G. Bae, F. Barlat, M.-G. Lee, Evaluation of springback for DP980 S rail using anisotropic hardening models, Jom, 68 (2016) 1850–1857.

[44] J. Choi, J. Lee, H.J. Bong, M.-G. Lee, F. Barlat, Advanced constitutive modeling of advanced high strength steel sheets for springback prediction after double stage U-draw bending, International journal of solids and structures, 151 (2018) 152–164.

[45] K. Lawanwong, H. Hamasaki, R. Hino, F. Yoshida, Double-action bending for eliminating springback in hat-shaped bending of advanced high-strength steel sheet, The International Journal of Advanced Manufacturing Technology, 106 (2020) 1855–1867.

[46] J. Choi, J. Lee, H.J. Bong, M.-G Lee, J. Ha, F. Barlat, Bulge bottoming process for reducing springback in U-bending of 980 MPa high-strength steel, International Journal of Material Forming, 18 (2025) 23.

[47] J.H. Schmitt, E. Aernoudt, B. Baudelet, Yield loci for polycrystalline metals without texture, Materials Science and Engineering, 75 (1985) 13-20.

[48] S. Yoon, F. Barlat, Non-iterative stress projection method for anisotropic hardening, Mechanics of Materials, 183 (2023) 104683.

[49] S.-Y. Lee, S.-Y. Yoon, J.-W. Kim, F. Barlat, K.-S. Oh, Evaluation of loading-path-dependent constitutive models for springback prediction in martensitic steel forming, International Journal of Mechanical Sciences, 251 (2023) 108317.

[50] K. Jeong, K.-H. Kim, S.-Y. Lee, H.J. Bong, S. Yoon, J. Yoon, Effect of path-dependent plasticity on springback in reverse bending and its application to roll forming, International Journal of Solids and Structures, 305 (2024) 113079.

[51] J.-Y. Lee, M.-G. Lee, F. Barlat, K.-H. Chung, D.-J. Kim, Effect of nonlinear multi-axial elasticity and anisotropic plasticity on quasi-static dent properties of automotive steel sheets, International Journal of Solids and Structures, 87 (2016) 254–266.

[52] Y. Choi, J. Lee, S.S. Panicker, H.-K. Jin, S.K. Panda, M.-G. Lee, Mechanical properties, springback, and formability of W-temper and peak aged 7075 aluminum alloy sheets: Experiments and modeling, International Journal of Mechanical Sciences, 170 (2020) 105344.

[53] A. Pasquale, V. Champaney, Y. Kim, N. Hascoët, A. Ammar, F. Chinesta, A parametric metamodel of the vehicle frontal structure accounting for material properties and strain-rate effect: application to full frontal rigid barrier crash test, Heliyon, 8 (2022).